RASĀYAN *J. Chem.*
Vol. 19 | No. 1 | 159-166 | January-March | 2026
ISSN: 0974-1496 | e-ISSN: 0976-0083 | CODEN: RJCABP
http://www.rasayanjournal.com
http://www.rasayanjournal.co.in

EXPLORING THE PHOTOVOLTAIC POTENTIAL OF QUINONE-BASED D–Π–A DYES: A COMPUTATIONAL STUDY OF THIOPHENE-LINKED ARCHITECTURES

R. Singh and M. Guin✉
Department of Chemistry and Biochemistry, Sharda University, Greater Noida-201310, India
✉Corresponding author: mridula.guin@sharda.ac.in

ABSTRACT

In this work, computational design and evaluation of three donor–π–acceptor (D–π–A) quinone-based dyes for photovoltaic applications was conducted. In the molecular framework, thiophene-based π-linkers (thiophene, dithienothiophene and thienothiophene) were combined with 2-hydroxy-1,4-benzoquinone as a donor and cyanoacrylic acid as an acceptor. Light-harvesting efficiency, density of states, UV-Vis absorption and frontier orbital gaps are investigated using Density Functional Theory (DFT) and Time-Dependent DFT (TD-DFT). The electronic distribution and charge-transfer behaviour were examined using transition density matrices and natural bond orbital analysis. Chemical reactivity descriptors such as ionisation potential, electron affinity, chemical hardness, and electronegativity were computed to understand stability and reactivity trends. Charge transport characteristics were studied through the calculation of reorganisation energies (λ_e and λ_h) and total λ, along with charge transfer integrals. Photovoltaic efficiency indicators such as open-circuit voltage (eV_{OC}), driving force for dye regeneration (ΔG^{reg}), and electron injection (ΔG^{inject}) were also analysed. According to the findings, the dye with an extended linker chain has better charge transport and optoelectronic characteristics is presumed to be an attractive option for dye-sensitised solar cell applications. Overall, these findings advance the understanding of quinone-based dye architectures and offer valuable design strategies that can guide future computational and experimental efforts toward improving photovoltaic performance.

Keywords: D–π–A Organic Dyes, Density Functional Theory, Optoelectronic Properties, Charge Transport, Reorganisation Energy

RASĀYAN*J. Chem.*, Vol. 19, No.1, 2026

INTRODUCTION

Environmental concerns and the growing demand for energy worldwide have prompted a great deal of research into sustainable energy sources, with solar energy emerging as a top contender. The most alluring photovoltaic technologies are dye-sensitised solar cells because of their low-cost simplicity of fabrication and ability to operate in diffuse light. DSSCs have been the subject of extensive research since the groundbreaking work of O'Regan and Grätzel in 1991.[1] Because it controls light absorption, electron injection and charge separation at the semiconductor interface, the sensitiser dye is crucial to the performance efficiency of DSSCs. Donor–π–acceptor (D–π–A) organic dyes are commonly used because they promote effective charge separation by facilitating directional electron transfer from the donor (D) to the acceptor (A) via a conjugated π-bridge. Key characteristics like charge transport, absorption properties, and frontier orbital energies can be systematically adjusted to improve DSSC efficiency by changing the donor, π-linker and acceptor units.[2] Although D-π-A dyes have been studied extensively, quinone-based donors, especially 2-hydroxy-1,4-benzoquinone, have not been studied much despite their strong electron-donating ability and structural rigidity. Extended conjugation and planarity are provided by thiophene-based π-linkers, which enhance charge delocalisation and optoelectronic performance.[3] Using cyanoacrylic acid as the acceptor and 2-hydroxy-1,4-benzoquinone as the donor, we created three new D–π A dyes by combining the three thiophene-based π-bridges (thiophene, thienothiophene and dithienothiophene) (Fig.-1). The evaluation of optoelectronic properties and important photovoltaic parameters was done using DFT and TD-DFT calculations. The effect of π-bridge extension on dye performance for DSSCs is systematically evaluated in this work.[4] Given the expense and difficulty of creating new dyes, computational techniques provide a strong tool for identifying potential compounds and forecasting important optoelectronic characteristics before they are confirmed experimentally. By

advancing the understanding of dye architectures for solar energy harvesting, this work contributes toward realising Sustainable Development Goal 7 (Affordable and Clean Energy), which emphasises innovation in sustainable energy materials and technologies.

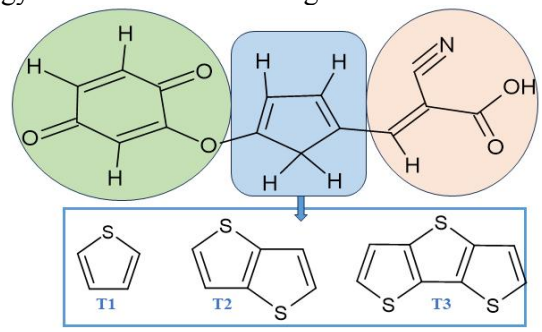

Fig.-1: Chemical Structure of the Studied Dyes with Three π-Linkers T1, T2, and T3

EXPERIMENTAL

Software called Gaussian 09 was used for all computations.[5] DFT was used to optimise ground-state geometries, and time-dependent DFT (TD-DFT) was used to calculate excited-state absorption properties. For DFT optimisation, the B3LYP functional was combined with the 6-31+G(d,p) basis set.[6] The stability of the optimised structures was confirmed by the absence of imaginary frequencies. The polarizable continuum model (CPCM) with self-consistent reaction field (SCRF) technique and the CAM-B3LYP functional were used to perform TD-DFT calculations with dichloromethane (DCM) as the solvent.[7]Multiwfn software was used to calculate Transition Density Matrix (TDM) plots, while GaussSum software was used to create Density of States (DOS) plots.

RESULTS AND DISCUSSION

Optimised Geometry and Frontier Molecular Orbitals

Figure-2 shows the optimised geometries, and Table-1 lists bond lengths (D_1 and D_2) and dihedral angles (Φ_1 and Φ_2) of the molecules. For all three dyes, the donor–linker bond length (D_1) remains nearly constant at ~1.36 Å, while the linker–acceptor bond length (D_2) ranges from 1.42 to 1.43 Å. The dihedral angles, Φ_1, vary from 90° to 95.5°, which helps suppress dye aggregation on the TiO_2 surface desirable feature. Interestingly, the Φ_2 values show significant variation: 81.2° for T1, 0.14° for T2, and 72.3° for T3. The near-planarity in T2 ($\Phi_2 \approx 0°$) suggests a more coplanar promoting stronger conjugation and potentially better intramolecular charge transfer (ICT) performance. In contrast, higher Φ_2 values in T1 and T3 imply more twisted geometries, which might reduce conjugation efficiency but could help minimise aggregation or undesired charge recombination.[6-7]

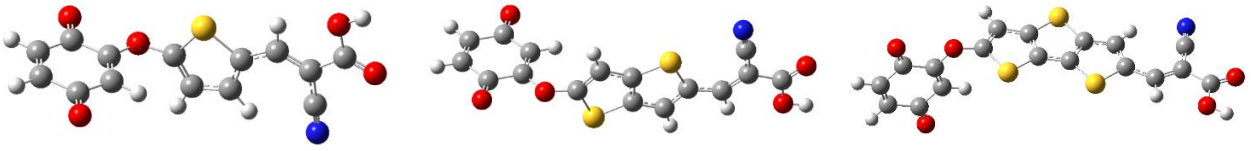

T1 T2 T3

Fig.-2: Gas Phase Optimised Geometry in the Ground State of the Designed Dyes

Table-1: The Dyes Optimal Dihedral Angles and Bond Distances for the Chosen Bonds

Molecules	D1/Å	D2/Å	Φ1(°)	Φ2(°)
T1	1.36	1.43	90.1	81.2
T2	1.36	1.42	97.4	0.14
T3	1.36	1.42	95.4	72.3

The lowest unoccupied molecular orbital (LUMO) and the highest occupied molecular orbital (HOMO)orbitals offer vital information on the optoelectronic behaviour of dye molecules, e.g. charge distribution and chemical stability across the dye structure. A reduced energy gap (ΔE) between HOMO

and LUMO generally improves ICT, which in turn improves solar cell performance [7]According to Fig.-3, the frontier molecular orbital analysis revealed that the HOMO is largely localised over the acceptor and π-linker segments, whereas the LUMO is predominantly distributed across the donor unit, indicating efficient photo-induced electron transfer potential.

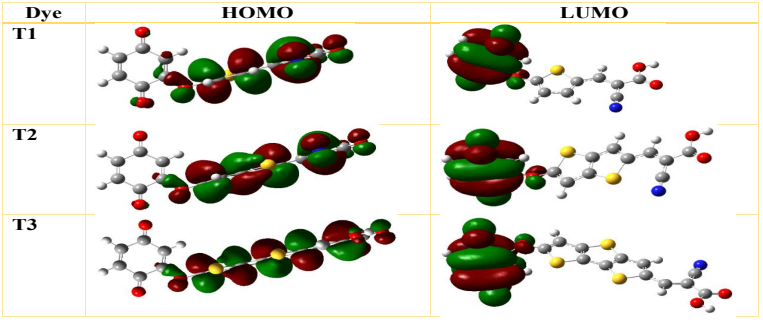

Fig.-3: Frontier Molecular Orbital Surface Plots of the Dyes

Chemical Reactivity Parameters

To further evaluate the electronic behaviour and stability of the designed dyes (T1–T3), global reactivity parameters like chemical potential (μ), electronegativity (χ), and chemical hardness (η) were calculated using the HOMO and LUMO energy values using equations-1, 2, and 3.[8-9]

$$\mu = \frac{E_{Lumo}+E_{Homo}}{2} \quad (1)$$

$$\chi = -\mu = \frac{-(E_{Lumo}+E_{Homo})}{2} \quad (2)$$

$$\eta = \frac{E_{Lumo}-E_{Homo}}{2} \quad (3)$$

The results are summarised in Table-2. Among the three dyes, T3 exhibits the lowest chemical hardness and smallest band gap, indicating enhanced charge transfer ability and high chemical softness, which are desirable features in solar cells. Conversely, T1, with the largest hardness, is expected to be more electronically stable but less reactive. These findings suggest that the gradual extension of the π-spacer increases electron delocalisation and improves charge transfer, as reflected in the lowering of χ and η values across T1 to T3.

Table-2: The Chemical and Electronic Parameter Values of the Studied Dyes.

Dyes	HOMO	LUMO	ΔE	χ	μ	η	IP_v	EA_v	IP_a	EA_a	ω^+	ω^-	ω
T1	-6.87	-3.94	2.93	5.40	-5.40	1.46	6.80	3.94	6.44	4.21	10.19	15.51	12.71
T2	-6.5	-3.93	2.57	5.21	- 5.21	1.28	6.50	3.93	6.15	4.18	11.08	16.24	13.54
T3	-6.23	-3.92	2.31	5.07	-5.07	1.15	6.20	3.92	5.98	4.14	11.50	16.42	13.91

In dye-sensitised solar cells (DSSCs), the sensitiser dye achieves two goals: it first introduces an excited electron into TiO_2, and it then extracts an electron from the electrolyte to fill the resulting hole. The dye's ability to acquire and lose electrons or holes determines how well charges are transferred, so understanding its ionisation potential (IP) and electron affinity (EA) provides crucial information. Equations-4 and 5 show how Koopmans' theorem was applied to determine the IP and EA using the HOMO and LUMO energy levels.[9-10]

$$IP = -E_{Homo} \quad (4)$$

$$EA = -E_{Lumo} \quad (5)$$

Additionally, an adiabatic approach was employed to estimate more accurate values of IP and EA, as described in Equations-6 and 7. This approach involved computing the molecular energies of the neutral and corresponding ionic species at the same level of theory.[10-11]

$$IP = E_{cation} - E_{Neutral} \quad (6)$$

$$EA = E_{Neutral} - E_{Anion} \quad (7)$$

The parameters of chemical reactivity can be used to evaluate the stabilisation energies. To better understand the dyes' electrical behaviour, equations 8 to10 was used to calculate the electrophilicity index (ω), electron-accepting power (ω^+) and electron-donating power (ω^-). Greater stability results from a higher ω^+ and higher ω, both of which indicate improved electron-accepting capacity and are therefore preferred for effective dyes. A list of the significant calculated values is given in the Table-2.[8-11]

$$\omega^+=\frac{(IP+3EA)^2}{16(IP-EA)} \quad (8)$$

$$\omega^-=\frac{(3IP+EA)^2}{16(IP-EA)} \quad (9)$$

$$\omega=\frac{(IP+EA)^2}{4(IP-EA)} \quad (10)$$

The computed chemical reactivity parameters shed light on the stability and electron transfer properties of the intended dye molecules. T3 exhibits the lowest ionisation potential (both adiabatic and vertical) of the three molecules, indicating its potential to lose electrons more readily. Notably, T3 exhibits the highest electron-accepting power (ω^+ =11.50) and electrophilicity index (ω = 13.91), demonstrating a superior capacity to stabilise additional charges.

Natural Bond Orbital (NBO) Analysis

Natural Bond Orbital (NBO) analysis was carried out to have a glimpse of how charge is localised and transferred among the three segments, e.g. donor, π-linker, and acceptor in the designed dye molecules. The computed NBO charges for each fragment are summarised in Table-3. In the donor segments, strong electron-donating behaviour was confirmed by their constant positive NBO charges. On the other hand, the π-linkers displayed negative charges, emphasising their function as pathways that conduct electrons. Additionally, the acceptor units had negative charges, which demonstrated their ability to draw electrons from the excited dye and transfer them into the TiO_2 conduction band. [12]Among the systems under investigation, T3 dye showed the greatest Δq^{D-A} (natural charge difference) between the acceptor and donor moieties. This suggests that, in contrast to T1 and T2, T3 facilitates better electron delivery to the anchoring site and more efficient charge separation.

Table-3: The Ground State NBO Analysis, where q^{Donor}, q^{Linker}, and $q^{Acceptor}$ represent the Total Natural Chargeon the Donor, Linker and Acceptor Groups, respectively

NBO parameters	T1	T2	T3
q^{Donor}	0.47	0.21	0.68
q^{linker}	-0.09	-0.08	-0.07
$q^{Acceptor}$	-0.11	-0.12	-0.14
Δq^{D-A}	0.58	0.33	0.82

Absorption Properties

The UV–visible absorption properties of the suggested dyes were examined using TD-DFT calculations. A summary of the main optical characteristics is given in Fig.-4. Note that the light-harvesting efficiencies (LHE) of DSSCs are a significant determinant of their performance. In general, a large quantity of photocurrent is produced by a large LHE. The LHE is calculated as $1-10^{-f}$.[13]As shown in Fig.-4, T3 shows the strongest peak at 404.04 nm followed by T2 (401.1 nm) and T1 (399.54 nm). The observed bathochromic shift in T3 indicates enhanced π-conjugation and more effective ICT, contributing to its superior optoelectronic characteristics. T2 exhibits noticeably greater oscillator strength and LHE than T1 and T3, indicating a greater chance of an electronic transition and enhanced photon absorption efficiency. All dyes undergo electronic transitions, primarily between the HOMO and LUMO or closely related orbitals.[14] Notably, the percentage contribution index (% CI) indicates that in T3, a more distributed transition density occurs across multiple orbital transitions, which further supports enhanced ICT and charge delocalisation. Overall, these optical parameters establish T3 exhibiting a broader and more intense absorption profile, lower excitation energy, and greater transition efficiency.

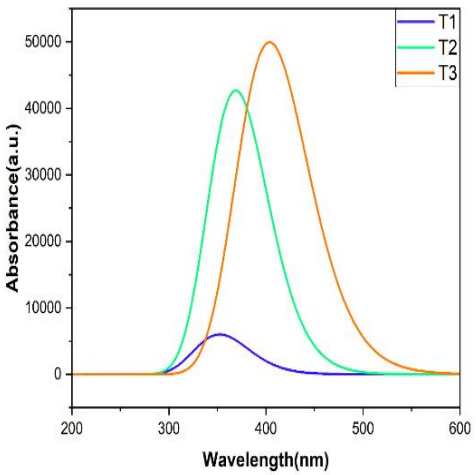

Dyes	E_{exc} (eV)	λ_{max} (nm)	Transition and % C.I.	f_0	LHE
T1	3.10	399.54	Homo-3→ Lumo (91.49)	0.0001	0.0002
	3.31	373.94	Homo-4→Lumo (92.66)	0.0002	0.0004
	3.51	352.41	Homo-1→Lumo (41.25)	0.14	0.27
T2	3.09	401.1	Homo-3→ Lumo (69.22)	0.0003	0.006
	3.30	375.08	Homo-5→Lumo (78.23)	0.0021	0.004
	3.61	368.86	Homo-2→Lumo (94.01)	1.05	0.911
T3	3.06	404.04	Homo→ Lumo+1 (58.19)	0.71	0.80
	3.07	403.3	Homo→Lumo+1 (42.93)	0.51	0.69
	3.26	379.67	Homo→Lumo (41.70)	0.0003	0.0006

Fig.-4: UV–Visible Absorption Spectra Graph of the Dyes and Summary of the Key Optical Properties

Density of States

Important details regarding the charge transport distribution characteristics of the dyes are provided by the density of states (DOS). GaussSum software is used in Fig.-5 to display the DOS graph of the three dye molecules.[15] The DOS plots display the distribution of virtual (red) and occupied (green) molecular orbitals.[16] All three dyes exhibit distinct HOMO–LUMO gaps. Interestingly, the virtual orbital peaks (LUMO and above) are compactly grouped close to the Fermi level (0 eV), especially for T3, indicating improved electron injection capability and increased electron affinity. Additionally, the DOS intensity rises from T1 to T3, particularly in the vicinity of the frontier orbitals, suggesting enhanced orbital overlap and delocalisation.

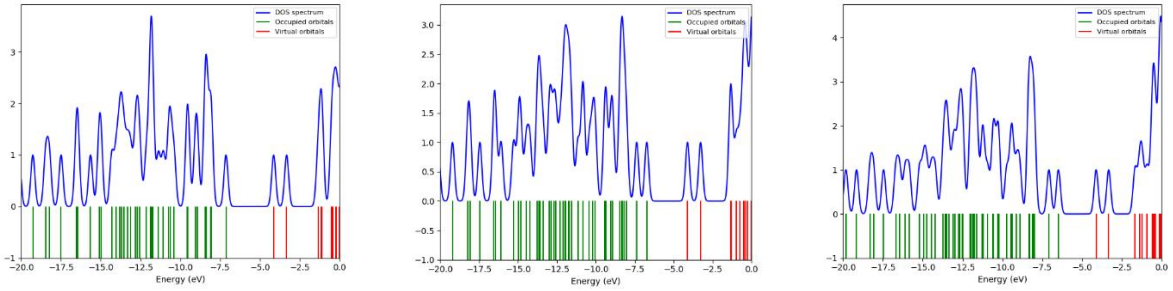

T1 T2 T3

Fig.-5: Graphical Presentation of Density of States (DOS) for the Studied Dyes

Transition Density Matrix

The TDM maps (Fig.-6) show electron–hole coherence, and the excitation behaviour of the dyes was calculated using Multiwfn software.[17] Charge separation is limited for T1 due to the weak donor–acceptor coupling, and excitation density is primarily located in donor–linker regions.[18]

Better electronic communication through the linker and more efficient charge transfer is indicated by T2, confirming enhanced ICT. T3 shows the strongest donor–acceptor delocalisation and the most extensive excitation coupling. Better charge separation, less recombination and increased charge mobility are indicated by its wider charge density distribution.

Photovoltaic Properties

Equation-11 is used to calculate the driving force for electron injection, where E^{dye*} Stands for the dye's excited state oxidation potential energy as determined by the eqn.-12. In this case, E^{dye} is the dye's ground state oxidation potential energy, which is the opposite of the E_{HOMO}.

For the semiconductor TiO_2, the conduction band (CB) reduction potential is E_{CB}($E_{CB} = -4.0$ eV) and the vertical transition associated with λ_{max} is $E_{0\text{-}0}$.

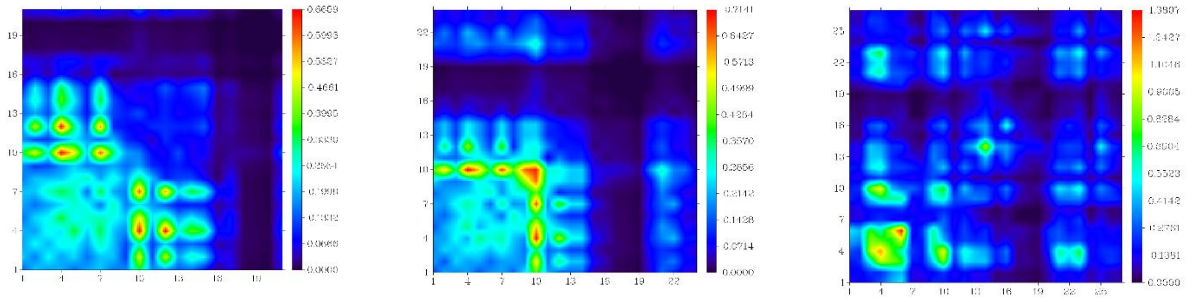

T1 T2 T3

Fig.-6: Transition Density Matrix (TDM) Map of the Dyes

$$\Delta G_{inj} = E^{dye*} - E_{CB} \quad (11)$$

$$E^{dye*} = E^{dye} - E_{0-0} \quad (12)$$

Using Eqn. 13 the driving force for dye regeneration is determined, where, $E^{electrolyte}_{Redox}$ is the redox potential of the electrolyteI^-/I_3^- (-4.85 eV) and eV_{OC} Can be evaluated according to eqn.-14.[19-20]

$$\Delta G_{reg} = E^{dye} - E^{electrolyte}_{Redox} \quad (13)$$

$$eV_{OC} = E_{LUMO} - E_{CB} \quad (14)$$

The hole (λ_h), electron (λ_e), and total (λ_{total}) reorganisation energy are evaluated using the total energies of the neutral, anionic and cationic species using standard methods.

Table-4: The Calculated Values of Photovoltaic Properties of Dyes (All values in eV)

Dyes	ΔG^{reg}	ΔG^{inject}	V_{OC}	λ_h	λ_e	λ_{total}
T1	2.02	-0.22	0.192	0.72	0.76	1.48
T2	1.65	-0.58	0.191	0.60	0.78	1.38
T3	1.38	-0.82	0.190	0.50	0.77	1.27

To assess the photovoltaic performance of the designed dyes, key parameters were calculated and are summarised in Table-4. The fact that all three dyes exhibit negative ΔG^{inject} values confirms the thermodynamic viability of electron injection. Among them, T3 exhibits the highest ΔG^{inject} value, implying the most efficient electron injection capability, followed by T2 and T1. Although all dyes show favorable ΔG^{reg} values, which measure how facile the regeneration process is, T1 has the highest ΔG^{reg} suggesting the fastest regeneration process. The open-circuit voltage (V_{OC}) remains nearly constant across all dyes, indicating an insignificant impact of linker modification on altering the energy gap between LUMO and CB of TiO_2. Reorganisation energies (λ_h, λ_e and λ_{total}) are vital for charge transport analysis. T3 displays the lowest hole reorganisation energy and the smallest total reorganisation energy, highlighting its potential for superior charge transport and photovoltaic performance. Overall, based on the combined analysis of ΔG^{inject}, ΔG^{reg} and reorganisation energies, T3 emerges as the most promising candidate among the three dyes. These results further reinforce the study's contribution to the Sustainable Development Goal 7 (Affordable and Clean Energy). By identifying and evaluating quinone-based dye architectures with enhanced charge-transfer characteristics, this work supports the advancement of cost-effective and sustainable materials for next-generation photovoltaic technologies.

CONCLUSION

In this study, three new D–π A organic dyes (T1, T2, and T3) were designed by systematically extending the π-conjugated linker with thiophene units to explore their potential in DSSCs. The computational results revealed that linker expansion led to improved planarity, reduced HOMO–LUMO gaps, enhanced intramolecular charge transfer, and superior light-harvesting ability as demonstrated by T3.

Key reactivity descriptors, including chemical hardness, ionisation potential, and electron affinity, confirmed the favourable electronic behaviour of T3. NBO, DOS, and TDM analyses consistently demonstrated more efficient charge separation and delocalisation in T3. Additionally, TD-DFT

simulations showed red-shifted and intense absorption spectra for T3, aligning with stronger oscillator strengths and better photovoltaic metrics (ΔG^{inject}, ΔG^{reg}, λ_h, λ_e). Overall, this work underscores the benefit of π-linker engineering specifically for thiophene-based molecules, which can significantly enhance the optoelectronic and photovoltaic performance of D–π A dyes. This study, therefore, contributes to the realisation of SDG 7 (Affordable and Clean Energy) by advancing the design of efficient, low-cost, and sustainable dye materials for next-generation solar energy conversion systems.

ACKNOWLEDGMENTS

The authors thank the Department of Chemistry and Biochemistry, Sharda University, for providing the computing facility and necessary infrastructure to accomplish this study.

CONFLICT OF INTERESTS

The authors declare that there is no conflict of interest.

AUTHOR CONTRIBUTIONS

The present work is related to *SDG-7: Affordable and Clean Energy*. All the authors contributed significantly to this manuscript, participated in reviewing/editing and approved the final draft for publication. The research profile of the authors can be verified from their ORCID ids, given below:

Riya Singh https://orcid.org/0000-0001-6011-768X
Mridula Guin https://orcid.org/0000-0003-2442-1646

Cite this article as: R. Singh and M. Guin, *Rasayan J. Chem.*, 19(1), 159-166(2026), https://doi.org/10.31788/RJC.2026.1919516.

REFERENCES

1. P. D. Sekaran and R. Marimuthu, *Brazilian Journal of Physics*, **54**, 28(2024), https://doi.org/10.1007/s13538-023-01375-w
2. G. Malta, J. Pina, J. C. Lima, A. J. Parola and P. S. Branco, *ACS Omega*, **9**, 14627(2024), https://doi.org/10.1021/acsomega.4c01201
3. O. Britel, A. Fitri, A. T. Benjelloun, M. Benzakour and M. Mcharfi, *Chemical Physics*, **565**, 111738(2023), https://doi.org/10.1016/j.chemphys.2022.111738
4. C. Liao, H. Wu, H. Tang, L. Wang and D. Cao, *Solar Energy*, **240**, 399(2022), https://doi.org/10.1016/j.solener.2022.05.043
5. M. J. Frisch, G. W. Trucks, H. B. Schlegel, et al., *Gaussian 16, Revision C.01*, Gaussian, Inc., Wallingford, CT (2016).
6. O. Britel, A. Fitri, Y. Sekkat, A. T. Benjelloun, M. Benzakour and M. Mcharfi, *Research Chemical Intermediate*, **50**, 5977(2024), https://doi.org/10.1007/s11164-024-05432-0
7. O. Britel, A. Fitri, A. T. Benjelloun, M. Benzakour and M. Mcharfi, *Structural Chemistry*, **34**, 1827(2023), https://doi.org/10.1007/s11224-023-02122-2
8. M. M. Fatma, A. L. K. Mahmoud, A. A. Abdel-Khalek and O. Kühn, *Computational Materials Science*, **226**, 112249(2023), https://doi.org/10.20944/preprints202305.1730.v1
9. M. Hachi, A. Slimi, A. Fitri, A. T. Benjelloun, M. Benzakour, M. Mcharfi, M. Khenfouch, I. Zorkani and M. Bouachrine, *Journal of Photochemistry and Photobiology A: Chemistry*, **407**, 113048(2021), https://doi.org/10.1016/j.jphotochem.2020.113048
10. J. K. Roy, S. Kar and J. Leszczynski, *ACS Sustainable Chemistry & Engineering*,**8**, 13328(2020), https://doi.org/10.1021/acssuschemeng.0c04061
11. Y. Li, X. Li and Y. Xu, *Spectrochimica Acta Part A: Molecular and Biomolecular Spectroscopy*, **234**, 118241(2020), https://doi.org/10.1016/j.saa.2020.118241
12. H. Roohi and N. Mohtamadifar, *RSC Advances*, **12**, 11557(2022), https://doi.org/10.1039/D2RA00906D

13. G. Fareed, R. Hussain, M. D. S. Haider, N. Kanwal, A. Hussain, M. Imran and M. A. Assiri, *Optical and Quantum Electronics*, **56**, 962(2024), https://doi.org/10.1007/s11082-024-06802-z
14. M. M. Ibrahim, N. M. El-Shafai, I. M. El-Mehasseb, S. N. Abdou and H. S. El-Sheshtawy, *International Journal of Energy Research*, **45**, 14804(2021), https://doi.org/10.1002/er.6755
15. N. M. O'Boyle, A. L. Tenderholt and K. M. Langner, *Journal of Computational Chemistry*, **29**, 839(2008), http://dx.doi.org/10.1002/jcc.20823
16. S. A. Siddique, M. Arshad, S. Naveed, M. Y. Mehboob, M. Adnan, R. Hussain, B. Ali, M. B. A. Siddique and X. Liu, *RSC Advances*, **11**, 27570(2021), https://doi.org/10.1039/D1RA04529F
17. T. Lu and F. Chen, *Journal of Computational Chemistry*, **33**, 580(2011), https://doi.org/10.1002/jcc.22885
18. M. Bilal Ahmed Siddique, R. Hussain, S. Ali Siddique, M. Yasir Mehboob, Z. Irshad, J. Iqbal and M. Adnan, *ChemistrySelect*, **5**, 7358(2020), https://doi.org/10.1002/slct.202001989
19. J. Zhang, H. C. Zhu, R. L. Zhong, L. Wang and Z.M. Su, *Organic Electronics*, **54**, 104(2018), https://doi.org/10.1016/j.orgel.2017.12.023
20. R. Maragani, R. Misra, M. S. Roy, M. K. Singh and G. D. Sharma, *Physical Chemistry Chemical Physics*, **19**, 8925(2017), https://doi.org/10.1039/C7CP00612H

[RJC-9516/2025]